Journal of Applied Polymer Science

Study on the morphology, static and dynamic mechanical properties of (styrene butadiene rubber/ethylene propylene diene monomer/ organoclay) nanocomposites vulcanized by the gamma radiation

Aida Shoushtari Zadeh Naseri, Azam Jalali-Arani
Department of Polymer Engineering & Color Technology, Amirkabir University of Technology, Tehran, Iran
Correspondence to: A. Jalali-Arani (E-mail: ajalali@aut.ac.ir)

ABSTRACT: Blends of styrene-butadiene rubber/ethylene–propylene-diene monomer (SBR/EPDM) with and without organoclay (OC) were prepared by melt mixing method. Then the samples were vulcanized by gamma radiation in comparison to conventional sulfur curing system. Characterization by X-ray diffraction analysis, atomic force microscopy, and Field emission scanning electron microscopy revealed the intercalation structure and good dispersion of the OC in prepared nanocomposites. In addition to this, by increasing the absorbed dose of radiation and using OC, reduction in solvent uptake, increase in crosslink density and improvement of mechanical and dynamic–mechanical properties were observed. Comparison of the tensile strength of irradiated nanocomposite with the sulfur cured one's displayed the synergistic effect of the OC and gamma radiation on tensile properties of SBR/EPDM blend. Mooney–Rivlin plot confirmed the increase in crosslink density and interaction between rubbers due to presence of OC and increasing absorbed dose. © 2016 Wiley Periodicals, Inc. J. Appl. Polym. Sci. **2016**, *133*, 43581.

KEYWORDS: blends; clay; elastomers; irradiation; mechanical properties

Received 17 August 2015; accepted 21 February 2016
DOI: 10.1002/app.43581

INTRODUCTION

To improve the properties of rubber compounds, reinforcing materials such as carbon black (CB) and silica are used extensively. Recently a great attention has been paid to replace them with nanoparticles in particular nanoclay.[1–5] The layered structure of nanoclay provides higher surface area for polymer chains to interact with, therefore using a small quantity of nanoclay results in higher performance properties as well as a lower weight of the product.[6–10]

Clay is a naturally occurring material with a hydrophilic nature and composed primarily of fine-grained minerals.[11] The hydrophilic clay mineral needs to be modified to improve its compatibility with the hydrocarbon matrices.[12–15] Therefore, the clays are modified with various alkylammonium salts to render the clay mineral hydrophobic at the surface and improves its compatibility with the organic molecules. This modification also expands the interlayer spaces of the clay.[16] Among the variety of natural occurring clays, sodium montmorillonite clay (Na-MMT) due to its high cation exchange capacities, large surface area, and good surface reactivity is a good candidate to be used with rubber matrices. This material is modified with different amounts of various alkylammonium and the modified clays are supplied with different trade names. The use of organo modified clay (OC) in styrene butadiene rubber (SBR)[17–19] and ethylene propylene diene monomer (EPDM)[13,14,20] has been reported. For instance, Meneghetti *et al.*[19] used different OC to reinforce SBR and reported that the surfactant chain length and its functional groups were the factors which affected the clay layers dispersion. Bhattacharya *et al.*[21] investigated the effect of different nanofillers on mechanical properties of the SBR based nanocomposites. They reported that by 6 phr loading of modified montmorillonite (Closite 15A), the modulus and tear strength of the compound were increased by 101 and 79%, respectively. The effect of clay modification on the structure and mechanical properties of EPDM/montmorillonite nanocomposites was studied by Zheng *et al.*[13] They used alkylamine containing hydroxyl groups to modify clay and reported a higher glass transition temperature for EPDM nanocomposite in comparison to gum EPDM vulcanizate. Ahmadi *et al.*[20] employed OC as opposed to pristine clay in EPDM. They reported that the use of OC results in an increase in the mechanical and thermal properties. For instance, by loading the same content of OC and pristine clay, the tensile strength of the EPDM/OC nanocomposite was about 60% higher than that of the EPDM/pristine clay composite.

Elastomeric materials are usually vulcanized by conventional chemical curing agents, to improve their physical and

mechanical properties. However, radiation curing method has recently received a great deal of attention,[22–27] due to the low operation cost, additive free technique, and its ability to produce more homogenous crosslink networks in the elastomer/elastomer blends. In addition, since the radiation curing is performed at room temperature, the release of toxic materials decreases, therefore this method is known as an environmentally friendly technique. Ahmed *et al.*[22] used the gamma radiation technique to vulcanize the elastomeric polymers. They compared the thermal stability of acrylonitrile butadiene rubber (NBR) and styrene butadiene rubber (SBR) vulcanizates cured by the sulfur, peroxide, and gamma radiation and reported much higher thermal stability for the irradiated samples. This was attributed to the uniformly distributed crosslinks and enhanced crosslink density in the radiation cured vulcanizates in comparison to the conventional cured samples. Abadchi and Jalali-Arani employed gamma radiation to prepare polybutadiene nano rubber powder[26] and used the prepared nanoparticles in blend with polypropylene (PP) to improve its impact strength.[28] Manshaie *et al.*[29] used electron beam radiation to vulcanize blends of natural rubber (NR) and SBR and investigated the dependence of vulcanizate physical–mechanical properties on absorbed dose. They reported that using a higher absorbed dose improved the properties such as oil resistance and heat stability of the final product.

Commonly, blending of elastomers is considered as an economical method to prepare new materials with improved processing and properties. Among the elastomeric blends, the blends of SBR and EPDM are of the special interest because incorporation of EPDM in SBR is expected to impart significant heat and ozone resistance to the SBR. On the other hand, weak adhesion, poor tear strength and high cost of the EPDM can be improved by the use of SBR.[27,30,31]

In this work, SBR/EPDM blends with and without OC are prepared and vulcanized with the gamma radiation system in comparison to the sulfur curing. The effects of the OC, curing system and the absorbed dose, on the morphology, static, and dynamic mechanical properties of the samples are investigated and discussed.

EXPRIMENTAL

Materials

Styrene-butadiene rubber with a Mooney viscosity of ML (1 + 4) 125 °C = 55 and styrene content of 23.5% (SBR1502, Bandare-Imam Co, Iran) and ethylene–propylene-diene monomer (EPDM, Vistalon 7000, Germany) with a Mooney viscosity ML (1 + 4)125 °C = 59 were used as the rubber matrix. Organoclay (Cloisite 15A) was purchased from Southern Clay Products (Gonzales, TX). This organoclay has been modified by dimethyl dehydrogenated tallow quaternary ammonium with a concentration of 125 meq/100 g of clay. Tetramethyl thiuram disulfide (TMTD) and 2,2 dibenzothiazyl disulfide (MBTS) from Bayer Company (Germany) were used as the accelerators. The other ingredients used in the compounds included stearic acid (Unichema, The United States), sulfur and ZnO (from a local factory, Iran). Analytical-grade of toluene (Merck) was used as the solvent.

Sample Preparation

To prepare samples for radiation curing, a blend of SBR/EPDM (50/50) with and without OC was mixed on an open two-roll mill at a temperature of 100 °C for about 12 min. Then a sheet form of the prepared compound was irradiated in the range of 0–150 kGy doses with an absorbed dose rate of 3.5 kGy/h in a gamma chamber with a Co-60 γ source. The prepared samples by this method are named as SE-RX (without OC) and SEOC-RX (with OC). R and X (0, 50, 100, and 150) denote the radiation curing system and the absorbed dose, respectively.

On the other hand, for preparation of a compound containing the sulfur curing system, similar to the previous steps, a blend of SBR/EPDM (50/50) was initially mixed with 5phr OC, 5 phr of zinc oxide (ZnO), and 1 phr stearic acid (St-A) on the two-roll mill at a temperature of 100 °C for 12 min. Then a conventional sulfur curing system consisting of sulfur (2 phr), and accelerators (1.5 phr) was added to the compound temperature of 40 °C. The optimum curing time of the compound was determined according to the ASTM 5289 test method, by means of an oscillating disk rheometer (ODR, Monsanto 100S UK). The compound was then vulcanized in a hydraulic hot press at a temperature of 155 °C. The prepared samples vulcanized by the sulfur curing system are denoted as the SE-S (unfilled sample) and SEOC-S (containing OC) in the result section.

Characterizations

X-ray Diffraction (XRD) Analysis. XRD analysis was performed by means of a Philips model X' Pert (Netherlands) equipment with CuKα radiation ($\lambda = 1.54056$°A) in a range from 1° to 10° and the step size of 0.02°/s at 30 mA and 40 kV. The d-spacing of the silicate layers was calculated using Bragg's equation ($\lambda = 2d\sin 2\theta$).

Atomic Force Microscopy (AFM). AFM test was performed with a Dualscope/Rasterscope C26 (DME, Denmark) equipment in tapping mode on the thin film samples at an ambient condition of 25 °C.

Swelling Behavior and Crosslink Density. The swelling behavior of the vulcanizates was investigated according to ASTM D 471 test method. To do the test suitable specimen (1 × 1× 0.2 cm^3) of each sample was weighed in air to the nearest 1 mg, and the mass recorded as m_1. It was immersed in toluene at room temperature. Then the test specimen was periodically removed from the toluene and dipped quickly in acetone. The remaining acetone was removed from the specimen surface with filter paper. It was weighed and the mass was recorded as m_2.The solvent uptake of each sample as mass of solvent per unit dry weight of each sample was calculated by [eq. (1)]:

$$\text{Solvent uptake} = \frac{m_2 - m_1}{m_1}. \quad (1)$$

Crosslinking density was determined according to the Flory–Rehner equation [eq. (2)] and using equilibrium swelling data of the samples.[32]

$$\frac{1}{M_C} = -\frac{1}{2}\rho V_0[\ln(1-V_R) + V_R + \chi V_R^2)/(V_R^{\frac{1}{3}} - \frac{1}{2}V_R)] \quad (2)$$

where V_0 is the molar volume of toluene (106 g/cm^3), ρ is polymer density (the arithmetic mean value of the density of the

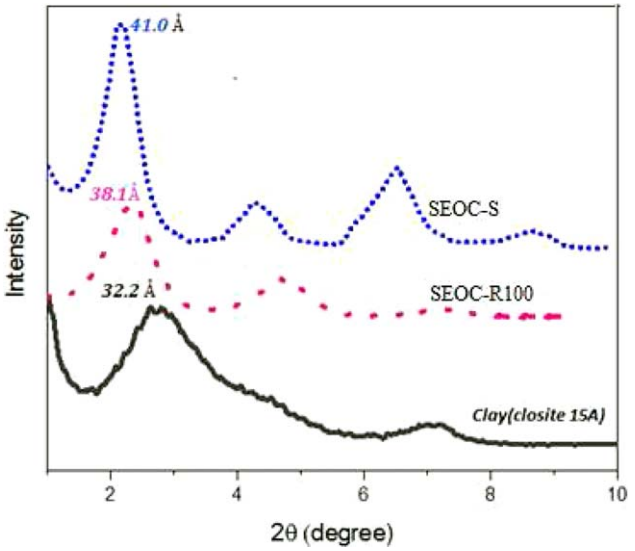

Figure 1. XRD patterns of the OC and the samples with OC, vulcanized by different curing systems. [Color figure can be viewed in the online issue, which is available at wileyonlinelibrary.com.]

SBR and EPDM), V_R is the volume fraction of rubber in the swollen sample, and χ (0.30033) is the polymer–solvent interaction parameter and is calculated using the eq. (3):

$$X=\beta+\frac{V_1}{RT}(\delta_s-\delta_p) \quad (3)$$

where δ_s and δ_p are the solubility parameters of the solvent and the polymer, β is the lattice constant whose value is taken as 0.34, R is the universal gas constant, and T is the absolute temperature.[33] The crosslink density is defined as $1/2M_C$.

Mechanical Properties. Tensile testing was carried out according to ASTM D412 test method, using a Galdabini Sun 2500 (Italy) at the strain rate of 500 mm/min. Hardness of the samples was determined according to ASTM D2240-A test procedure with a Shore A hardness tester (Karl Frank, Germany). The mean value of three tests is reported as the obtained results in this section.

Dynamic Mechanical–Thermal Analysis (DMTA). DMTA tests on the cured samples were performed using a Mettler Toledo TTDMA (The United Kingdom). DMTA spectra were taken in tension mode at 1 Hz frequency (linear-viscoelastic region) in a broad temperature range of −100 to +100 °C.

Field Emission Scanning Electron Microscopy (FE-SEM). FE-SEM equipment (Hitachi S-4160, Japan) was employed to investigate the compatibility between the composite components as well as the clay dispersion state. The test was carried out on the freeze fractured surface of the vulcanizates. The surface was coated with a thin layer of gold before the test.

RESULTS AND DISCUSSION

XRD Results

The XRD diffraction patterns of the OC and the samples containing OC are shown in Figure 1. The XRD pattern of the OC (Cloisite 15A) shows a broad peak at $2\theta = 2.734°$ corresponding to an interlayer space of 32.2 Å. It is observed that the peak shifts toward the smaller angles, $2\theta = 2.15°$ and $2\theta = 2.31°$ corresponding to interlayer spaces of 41.0 and 38.1 Å in the XRD patterns of the sulfur cured (SEOC-S) and radiation cured (SEOC-R) samples, respectively. This indicates the intercalation of the rubber chains into the interlayer spaces of the OC. The greater interlayer space of the OC in the SEOC-S, in comparison to that of SEOC-R, may be explained by this fact that a greater tension is applied on this compound during its melt mixing with curing materials and in compression molding process; these may cause a greater intercalation of the rubber chains. However, the curing materials (such as stearic acid) used in this compound have also the chance of intercalation in this compound.[34,35]

The appearance of the second and third peaks has also been reported and discussed in other works.[36–40] For instance, this was attributed to some collapsing of the OC layers due to de-intercalation of the amine modifier[36,37] and re-agglomeration of the silicate layers[37,38] during the melt mixing process. The presence of these peaks may also be attributed to the unmodified part of the clay as well as the higher order peak corresponding to d002[37] or the different arrangements of the substituent's of the compensating cations.[39]

Moreover, in the XRD pattern of both samples, a secondary peak is observed at the 2θ value in the range 4.2°–4.5° which indicates the clay agglomerations in these samples.

The presence of a third peak in the SEOC-S sample may be due to degradation or exiting of the clay platelets surface modifier during compound vulcanization in a hot press. This results in the collapsing of the clay layers and decreasing the interlayer distance of the OC.

AFM Results

Figure 2(a) shows the AFM image of the SE-R100 sample. Because the viscosity of the two phases SBR and EPDM are almost identical, they cannot be distinguished from each other in this image. Comparing this figure with the AFM image of the SEOC-R100 [Figure 2(b)], the latter displays a co-continuous morphology for the rubber phases and a good dispersion of the OC. The presence of some white features in Figure 2(b) can be attributed to the OC layers[41] dispersed in the SEOC-R100. This figure shows that the clay tends to be located in one of the phases. Since the SBR with a solubility parameter of about 17.46 $[(J/cm^3)^{1/2}]$[33] is more polar than the EPDM with a solubility parameter of about 15.95 $[(J/cm^3)^{1/2}]$[33] it is expected that the OC is located at the SBR; however, it is a hypothesis and needs more investigation. Nevertheless, this localization results in an increase in the viscosity of this phase; therefore, it can be distinguished from the other phase by the AFM test.

Swelling Behavior and Crosslink Density

The swelling behavior of the samples is shown in Figure 3. It can be seen that, increasing the absorbed dose results in reducing the ultimate solvent uptake and swelling rate. It can be explained that the increase in the absorbed dose increases the radicals' formation on the polymers backbone. The formed

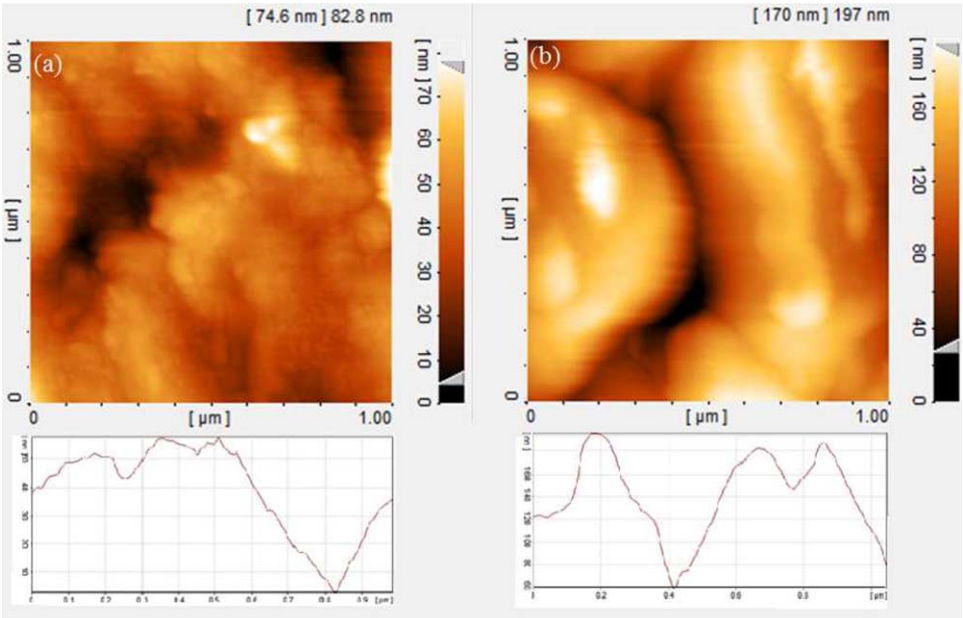

Figure 2. AFM photographs of (a) unfilled SE-R100 and (b) SEOC-R100 samples. [Color figure can be viewed in the online issue, which is available at wileyonlinelibrary.com.]

radicals on the two polymers backbone may react with each other and enhance the interaction and compatibility between the phases. This issue was also reported by Dubey *et al.*[42] On the hand the interaction between the formed radicals may lead to an increase in the crosslink density. The improvement of interaction between phases and also the increase in crosslink density reduces the solvent uptake by the polymer blend. It is noted that the effect of radiation on the chemical bonds formed during irradiation was explained in our previous work.[27]

A comparison between the swelling behavior of the samples containing OC with that of the corresponding unfilled blends displays that the use of OC results in a reduction in the amount of solvent up take. It can be explained that the impermeability and the layered structure of the OC through increasing the average diffusion path decrease the swelling rate and solvent uptake.[43] On the other hand it is expected that the use of OC increases the interaction between constituents of a sample and also causes an increase in crosslink density, which result in the decrease in the solvent uptake.

Table I presents the crosslink density of the samples. This table illustrates that the crosslink density of SE-RX samples is increased by increasing the absorbed dose. In addition to this, the crosslink density of the sample irradiated at the dose above 100 kGy, is higher than that of corresponding sulfur cured ones. Comparing the crosslink density of the nanocomposites to that of the corresponding unfilled blends depicts that the use of OC results in an increase in the crosslink density. The increase in crosslink density in sulfur cured samples due to the use of organoclay has been reported by many researcher and was attributed to participation of the intercalate (octadecylamine) of OC, in the curing reactions.[44–49] The increase in cross link density in OC/rubber nanocomposites cured by irradiation was also reported by Ali *et al.* and they attributed it to interaction of filler/matrix at the interface and formation of physical crosslinks.[50]

Mechanical Properties

In this section, the effects of OC incorporation, curing system and crosslink density on mechanical properties of prepared samples are investigated. The stress–strain curves of the unfilled compound and corresponding nanocomposite vulcanized at different absorbed doses are displayed in Figure 4(a). This figure shows that incorporation of 5 phr OC results in a significant increase in tensile strength which can be attributed to intercalation of rubber chains between the interlayer spaces of the clay layers and the interaction between rubber segments and surface modifier on the clay layers.

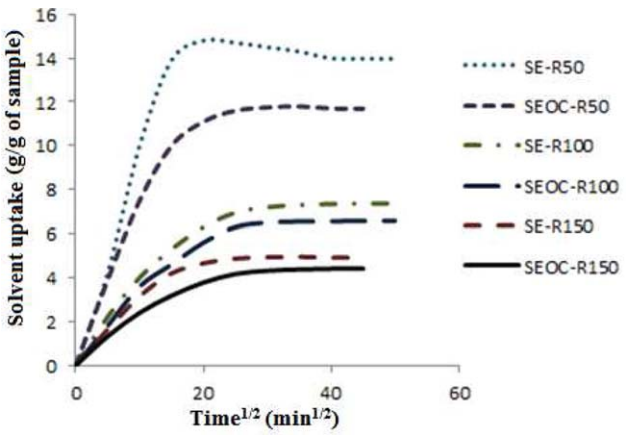

Figure 3. The solvent uptake as a function of time for the samples. [Color figure can be viewed in the online issue, which is available at wileyonlinelibrary.com.]

Table I. Crosslink Density of Irradiated and Sulfur Cured Samples

Unfilled samples	Crosslink density (mol/g) × 10^4	Nanocomposites	Crosslink density (mol/g) × 10^4
SE-R50	0. 203	SEOC-R50	0. 344
SE-R100	3.28	SEOC-R100	4.28
SE-R150	4.28	SEOC-R150	5.12
SE-S	3.45	SEOC-S	3.85

Moreover, comparing the stress–strain curves of SE-X compounds vulcanized at different absorbed doses exhibits that the increase in the absorbed dose leads to an improvement in mechanical properties such as tensile strength and modulus which is relevant to crosslinking density intensification (Table I). The same trend of improvement in tensile properties, due to increasing absorbed dose, can also be seen in the prepared nanocomposites. For example, tensile strength of the SEOC-R150 is about three folds of SEOC-R50's. Another remarkable point in Figure 4 is the effect of organoclay incorporation on elongation at break values. It is observed that at a constant absorbed dose (above 50 kGy) and having sufficient crosslinking density, the elongation at break of the samples is increased by adding OC to the system. This is attributed to the onset of a "secondary structure" being capable to dissipate the input energy upon uniaxial loading.[51] This structure is analogous to the so-called "secondary structure" of the CB appearing usually in highly filled rubbers. To attain such morphology at a

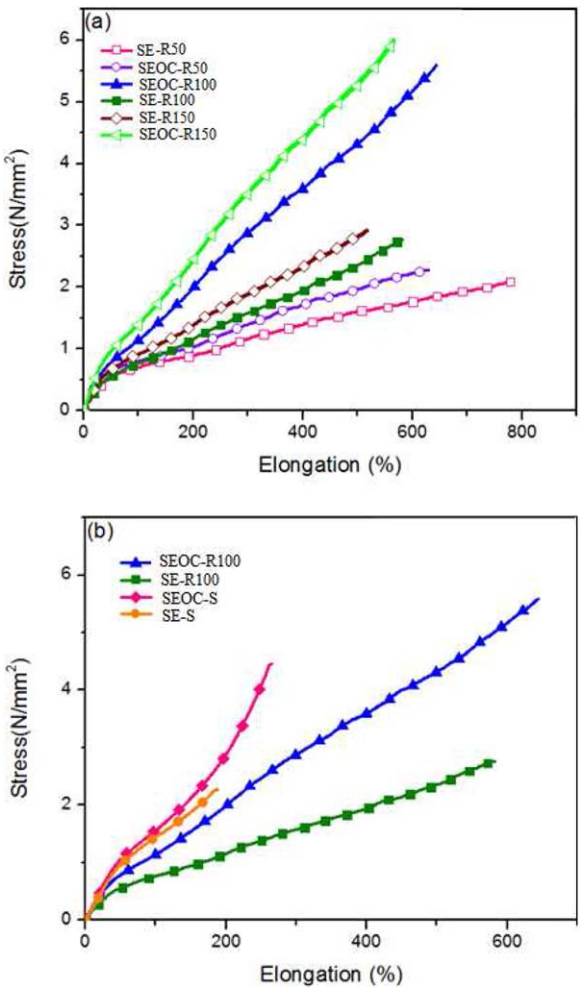

Figure 4. Stress–strain curves of (a) SE-RX and SEOC-RX vulcanized at different absorbed dose; (b) SE-R100 and SEOC-R100 compared with corresponding sulfur cured samples. [Color figure can be viewed in the online issue, which is available at wileyonlinelibrary.com.]

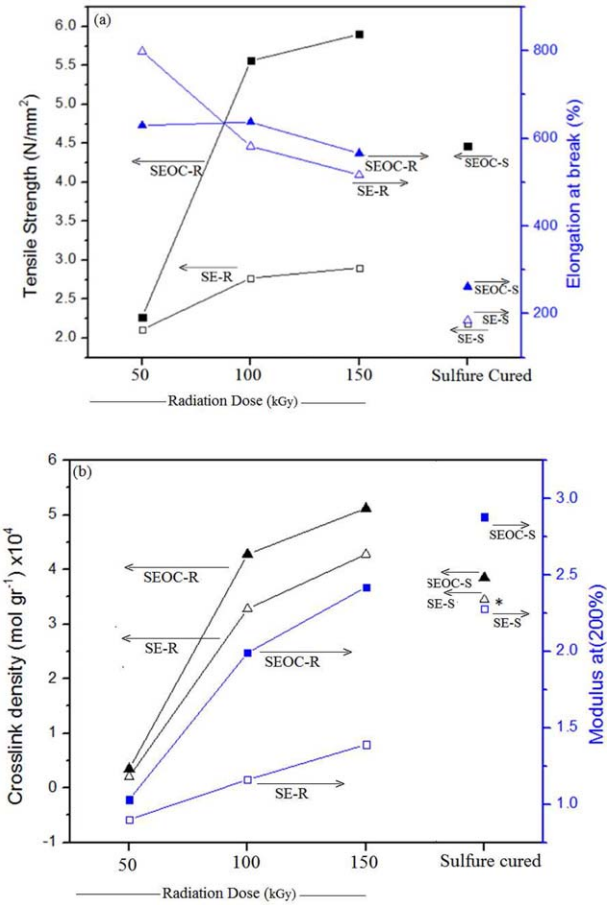

Figure 5. Comparing (a) tensile strength (*square symbols*) and elongation at break (*triangle symbols*) and (b) modulus at 200% (*square symbols*) and crosslink density (*triangle symbols*); of the unfilled (*open symbols*), and filled (*solid symbols*) samples cured by different radiation doses and sulfur cure system. *Since the sulfur cured unfilled sample was broken at elongation lower than 200%, therefore its modules (185%) at break is shown here. [Color figure can be viewed in the online issue, which is available at wileyonlinelibrary.com.]

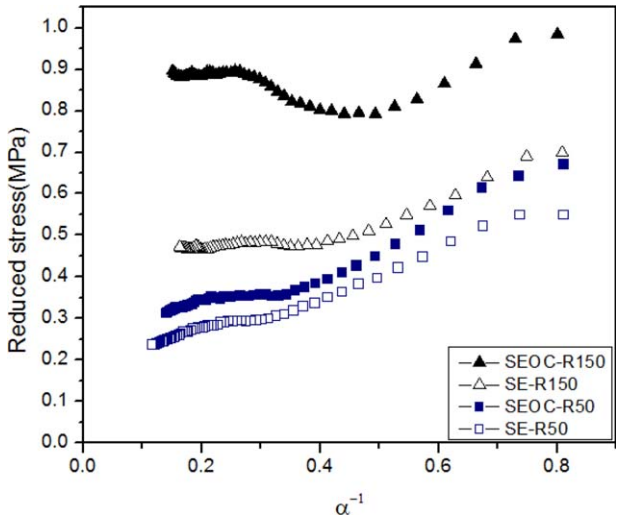

Figure 6. Reduced stress/α^{-1} of SE-RX and SEOC-RX samples. [Color figure can be viewed in the online issue, which is available at wileyonlinelibrary.com.]

Table II. The Values of C_1 and C_2

Sample code	C_1 (intercept)	C_2 (slope)
SE-R50	0.0971	0.6156
SEOC-R50	0.0993	0.7447
SE-R150	0.1213	0.7683
SEOC-R150	0.3924	0.7813

low organoclay content a good dispersion of the clay is required in the rubber matrix.[51]

Figure 4(b) shows the stress–strain curve of the radiation cured and sulfur cured samples. As can be seen, the radiation cured samples display a noticeable improvement in tensile strength and elongation at break values as compared with the sulfur cured ones. Comparing tensile strength and elongation at break of the SE-S sample with the SE-R100 one's, exhibits an enhancement of about 27 and 215% for them, respectively. The same comparison between SEOC-S and SEOC-R100 properties exhibits an enhancement of about 25 and 144% for the tensile strength and elongation at break, respectively for the latter system. It can be explained that the gamma radiation in addition to vulcanization causes more compatibility between the SBR and EPDM which leads to improvement of properties.[42]

Comparing the increase in tensile strength [Figure 5(a)] and modulus [Figure 5(b)] of nanocomposites (SEOC-R100 and SEOC-R150 samples) cured by gamma radiation or sulfur cure system (SEOC-S) with respect to that of corresponding unfiled samples, the synergistic effect of OC and gamma radiation on improvement of tensile strength and modulus can be seen. In addition to these, it can be seen in Figure 4(a) that in spite of increase in tensile strength and modulus these samples exhibit the same enhancement of elongation at break.

Comparing the modulus of different samples shown in Figures 4 or [5](b) displays a higher modulus for the sulfur cured samples as they are compared with corresponding radiation cure ones. This may be

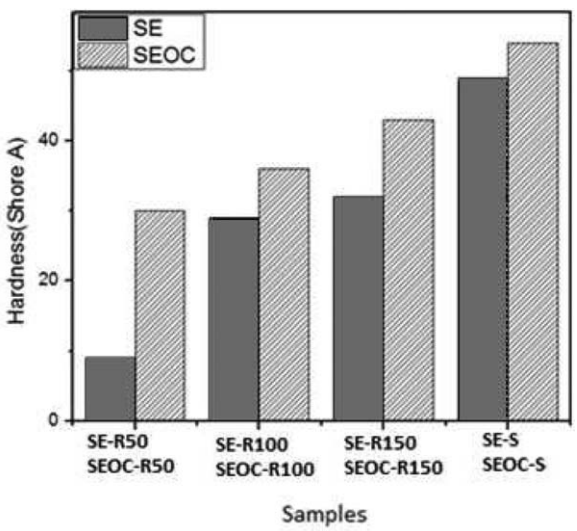

Figure 7. Hardness of irradiated and sulfur cured samples.

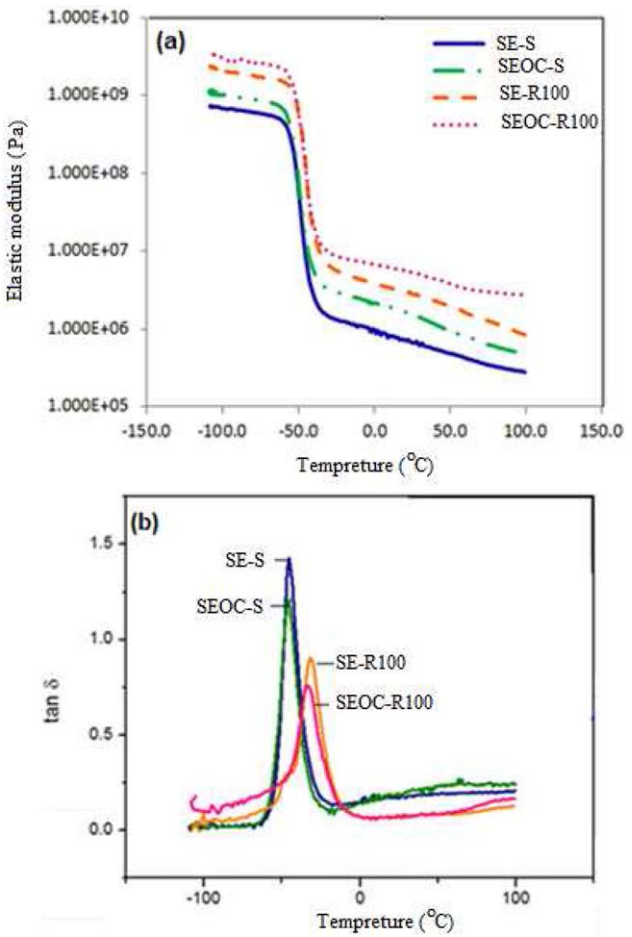

Figure 8. (a) Elastic modulus/temperature and (b) tanδ/temperature of the SBR-EPDM blend and its nanocomposites vulcanized by gamma radiation and sulfur curing systems. [Color figure can be viewed in the online issue, which is available at wileyonlinelibrary.com.]

Table III. Glass Transition Temperature and tanδ Value of the Samples

	Glass transition temperature (T_g)	tanδ
SE-S	−45.5	1.4275
SEOC-S	−45.5	1.2093
SE-R100	−32	0.9056
SEOC-R100	−35.9	0.7589

due to different crosslinking bonds formed in these samples. The crosslinking bonds formed in the sulfur cured samples are almost poly sulfide ones (Sx), while in the radiation cured samples the carbon—carbon (—C—C—) bonds are formed. It can also be seen that the more increase in the absorbed dose, the more intensification of the modulus which is related to a raise in crosslinking density.

For further investigation, the Mooney–Rivlin curves were plotted based on eq. (4).[52,53]

$$\frac{\sigma}{\alpha-\alpha^{-2}} = C_1 + C_2\alpha^{-1} \quad (4)$$

where σ is the applied stress, α is extension ratio and $\frac{\sigma}{\alpha-\alpha^{-2}}$ is known as reduced stress $(\sigma*)$ which is a measure of elastomer stiffness. The constant C_1 is a measure of the crosslink density and is given as the intercept at $\alpha^{-1}=0$. C_2 is the slope of a straight line in the Mooney–Rivlin plot and physical networks such as chain entanglements and interactions between filler particles and polymer–filler can contribute to its magnitude. Therefore, the plot of reduced stress $(\sigma*)$ versus inverse extension ratio (α^{-1}) can give useful data about the network structure and the flexibility of the network chains.

Figure 6 shows the reduced stress $(\sigma*)$ against inverse extension ratio (α^{-1}) of unfilled (SE-RX) and filled (SEOC-RX) samples irradiated at maximum (150 kGy) and minimum (50 kGy) doses. It can be seen that the obtained curves are found to be linear in the intermediate region. The value of C_1 and C_2 are reported in Table II.

It can be seen that the incorporation of OC as well as increase in absorbed dose results in an increase in both C_1 and C_2 values.

It is worth mentioning that the impact of OC content is more significant at lower absorbed dose on non-Gaussian aspect of the networks. This is due to improvement of radical–radical interaction and formation of physical crosslinks.[27,54] At higher absorbed dose the presence of OC significantly affects the C_1 values and represents its effect on the increase in crosslink density of the sample. Hardness of different samples is presented in Figure 7. It is observed that the hardness values of the samples follow a trend similar to the modulus which was explained above. The same explanation can be employed here for the variation of the hardness.

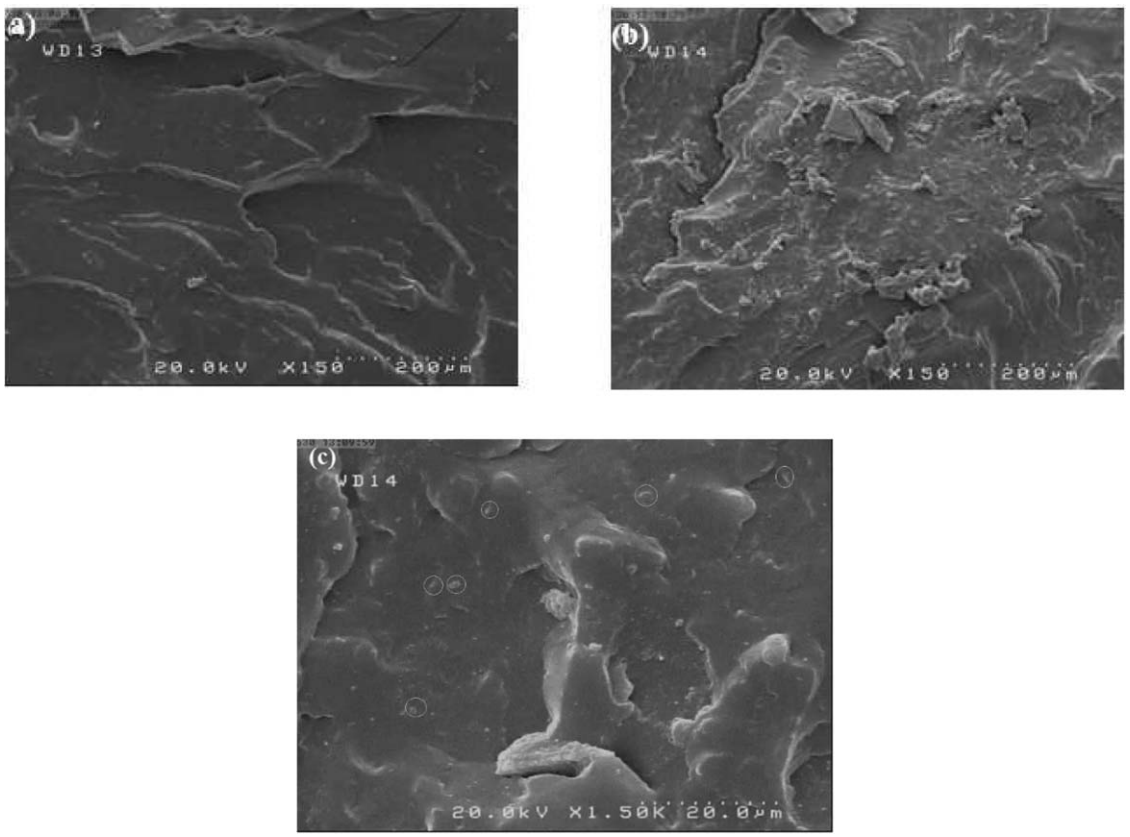

Figure 9. SEM micrograph of the fracture surface of (a) SEOC-S, (b) SEOC-R, (c) SEOC-S at different magnifications.

DMTA Results

Figure 8 demonstrates the dynamic elastic modulus (E') and the mechanical loss factor (tanδ) as a function of temperature for the SBR-EPDM blend and its nanocomposites vulcanized by gamma radiation and sulfur curing systems.

As can be seen in Figure 8(a), supplementing organoclay to the blends leads to an increase in the dynamic elastic modulus (E') in the glassy, glass transition, and rubbery regions. This may be related to the increase in CLD and possible intercalation of the rubber chains between the interlayer spaces of the OC. By intercalation of the rubber chains between the interlayer spaces of the OC, the effective volume fraction of the filler is increased and enhances the elastic modulus. Moreover, it is observed that the compounds cured by the gamma radiation, in comparison to their corresponding sulfur cured ones, show a higher dynamic elastic modulus. It can be explained that using gamma radiation improves the interaction between the polymer components in the compound through its capability to create radicals on the polymers backbone.

Figure 8(b) and Table III display that adding OC to the compound results in a moderate reduction of tanδ peak height in both nanocomposites either cured by the sulfur or gamma radiation. As discussed in the previous sections addition of OC resulted in a greater CLD in the compound. Therefore, the decrease in tanδ peak height in the samples with OC in comparison to that of corresponding unfilled samples, can be attributed to increase in CLD as well as the interaction between OC and rubbers and also the possible intercalation of the rubber chains between the interlayer spaces of the OC. The reduction in peak height due to adding OC has been reported in other articles.[55–57]

As the rubber chains are confined in the OC layers, the viscous motions of the chains are restricted and lead to an increase in the elastic response. Moreover, in comparing the DMTA results for the samples vulcanized by different curing systems, a significant reduction of tanδ peak is observed for the radiation cured samples, which can be related to the greater crosslink density and also higher compatibility between the phases in radiation cured samples. On other hand, Table I depicts no significant difference between crosslink density of the sample (SE-S) cured by the sulfur and that (SE-R100) was irradiated at 100 kGy. Therefore, it can be explained that, in this work, the higher compatibility between the phases due to irradiation has more effect on the reduction of tanδ peak. The higher glass transition temperature (T_g) of the radiation cured samples in comparison to corresponding sulfur cured ones (Table III), also confirms the higher compatibility of the components in the irradiated samples.

FE-SEM Results

The SEM micrograph of the fracture surface of SEOC-S and SEOC-R samples are shown in Figure 9(a,b), respectively. It can be seen that the fracture surface of SEOC-R is rougher than that of SEOC-S sample, which is attributed to their different failure mechanisms. The failure mechanism in the SEOC-S sample is through delamination occurred at the interface of clay platelets and the rubber matrix. This behavior is indicative of weak interfacial interaction (with respect to SEOC-R sample) between the clay and rubber matrix and results in a smooth fracture surface. On the other hand, a rough fracture surface of the SEOC-R sample as compared with that of SEOC-S exhibits more compatibility between phases in this sample. This can be attributed to the compatibilization effect of gamma radiation. The SEM micrograph illustrated in Figure 9(c) shows that the clays are well dispersed in the rubber matrix.

CONCLUSIONS

In this work, SBR/EPDM blends and their nanocomposites (EPDM/SBR/OC) were prepared and vulcanized by the gamma radiation and sulfur cure system. Characterization and measuring properties of the samples displayed an intercalation structure and good dispersion of the OC. Incorporation of 5 phr of the OC resulted in a significant increase in tensile strength and elongation at break of the samples. By the way obtained results showed that the solvent resistance and tensile strength were improved by increasing the absorbed dose. Mooney–Rivlin plot confirmed the increase in crosslink density and interaction between rubbers due to presence of OC and increasing absorbed dose. The DMTA analysis showed a reduction in the height of the tanδ/temperature peak for the nanocomposites in comparison to their corresponding unfilled blends. A similar variation of tanδ/temperature peak height was observed for the radiation cured sample in comparison to sulfur cured one's, which was attributed to the compatibilization effect of the gamma radiation.

ACKNOWLEDGMENTS

The authors would like to express their thanks to the Iran Nanotechnology Initiative Council for funding assistance.

REFERENCES

1. Maiti, M.; Bhattacharya, M.; Bhowmick, A. K. *Rubber Chem. Technol.* **2008**, *81*, 384.
2. Sadhu, S.; Bhowmick, A. K. *Rubber Chem. Technol.* **2003**, *76*, 860.
3. Wu, Y. P.; Ma, Y.; Wang, Y. Q.; Zhang, L. Q. *Macromol. Mater. Eng.* **2004**, *289*, 890.
4. Kooshki, M. M.; Jalali-Arani, A. *e-Polymers* **2009**, *9*, 1570.
5. Monfared, A.; Jalali-Arani, A. *Appl. Clay Sci.* **2015**, *108*, 1.
6. Arroyo, M.; Lopez-Manchado, M. A.; Herrero, B. *Polymer* **2003**, *44*, 2447.
7. Chan, M. L.; Lau, K. T.; Wong, T. T.; Ho, M. P.; Hui, D. *Composites Part B* **2011**, *42*, 1708.
8. Das, A.; Wang, D. Y.; Stöckelhuber, K. W.; Jurk, R.; Fritzsche, J.; Klüppel, M.; Heinrich, G. *Adv. Polym. Sci.* **2011**, *239*, 85.
9. Nematollahi, M.; Jalali-Arani, A.; Golzar, K. *Appl. Clay Sci.* **2014**, *97*, 187.
10. Monfared, A.; Jalali-Arani, A.; Mohammadi, N. *J. Macromol. Sci. Part B* **2014**, *53*, 918.

11. Bergaya, F.; Lagaly, G. Handbook of Clay Science; Elsevier: New York, **2013**; Vol. *5*, p 3.
12. Sadhu, S.; Bhowmick, A. K. *J. Appl. Polym. Sci.* **2004**, *92*, 698.
13. Zheng, H.; Zhang, Y.; Peng, Z.; Zhang, Y. *Polym. Test.* **2004**, *23*, 217.
14. Gatos, K. G.; Karger-Kocsis, J. *Polymer* **2005**, *46*, 3069.
15. El Achaby, M.; Ennajih, H.; Arrakhiz, F. Z.; El Kadib, A.; Bouhfid, R.; Essassi, E.; Qaiss, A. *Composites Part B* **2013**, *51*, 310.
16. Pavlidou, S.; Papaspyrides, C. D. *Prog. Polym. Sci.* **2008**, *33*, 1119.
17. Song, M.; Wong, C. W.; Jin, J.; Ansarifar, A.; Zhang, Z. Y.; Richardson, M. *Polym. Int.* **2005**, *54*, 560.
18. Zhang, H.; Wang, Y.; Wu, Y.; Zhang, L.; Yang, J. *J. Appl. Polym. Sci.* **2005**, *97*, 844.
19. Meneghetti, P.; Shaikh, S.; Qutubuddin, S.; Nazarenko, S. *Rubber Chem. Technol.* **2008**, *81*, 821.
20. Ahmadi, S. J.; Huang, Y.; Li, W. *Compos. Sci. Technol.* **2005**, *65*, 1069.
21. Bhattacharya, M.; Maiti, M.; Bhowmick, A. K. *Polym. Eng. Sci.* **2009**, *49*, 81.
22. Ahmed, S.; Basfar, A. A.; Aziz, M. A. *Polym. Degrad. Stabil.* **2000**, *67*, 319.
23. Banik, I.; Bhowmick, A. K. *Radiat. Phys. Chem.* **2000**, *58*, 293.
24. Dubey, K. A.; Bhardwaj, Y. K.; Chaudhari, C. V.; Bhattacharya, S.; Gupta, S. K.; Sabharwal, S. *J. Polym. Sci. Part B: Polym. Phys.* **2006**, *44*, 1676.
25. Samaržija-Jovanović, S.; Jovanović, V.; Marinović-Cincović, M.; Budinski-Simendić, J.; Marković, G. *Composites Part B* **2014**, *62*, 183.
26. Abadchi, M. R.; Jalali-Arani, A. *Nucl. Instrum. Meth. Phys. Res. Sect. B* **2014**, *320*, 1.
27. Naseri, A. S. Z.; Jalali-Arani, A. *Radiat. Phys. Chem.* **2015**, *115*, 68.
28. Abadchi, M. R.; Jalali-Arani, A. *Iran. Polym. J.* **2015**, *24*, 805.
29. Manshaie, R.; Khorasani, S. N.; Veshare, S. J.; Abadchi, M. R. *Radiat. Phys. Chem.* **2011**, *80*, 100.
30. Zhao, J.; Ghebremeskel, G.; Peasely, J.; Neches, P. *KGK. Kautschuk, Gummi, Kunststoffe* **2001**, *54*, 84.
31. El-Nashar, D. E. *Polym. Plast. Tech. Eng.* **2005**, *43*, 1425.
32. Flory, P. J. Principles of Polymer Chemistry; Cornell University Press: United States, **1953**, p 432.
33. Hansen, C. M. Hansen Solubility Parameters: A User's Handbook; CRC Press: Boca Raton, **2007**, p 493.
34. Ma, Y.; Li, Q. F.; Zhang, L. Q.; Wu, Y. P. *Polym. J.* **2007**, *39*, 48.
35. Das, A.; Stöckelhuber, K. W.; Jurk, R.; Jehnichen, D.; Heinrich, G. *Appl. Clay Sci.* **2011**, *51*, 117.
36. Benali, S.; Peeterbroeck, S.; Larrieu, J.; Laffineur, F.; Pireaux, J. J.; Alexandre, M.; Dubois, P. *J. Nanosci. Nanotechnol.* **2008**, *8*, 1707.
37. Sharif, J.; Wan Yunus, W. M. Z.; Zaman, K.; Ahmad, M. B. *Polym. Test.* **2005**, *24*, 211.
38. Sadhu, S.; Bhowmick, A. K. *J. Polym. Sci. Part B: Polym. Phys.* **2004**, *42*, 1573.
39. Galimberti, M.; Coombs, M.; Cipolletti, V.; Riccio, P.; Riccò, T.; Pandini, S.; Conzatti, L. *Appl. Clay Sci.* **2012**, *65*, 57.
40. Sadeghi Ghari, H.; Jalali-Arani, A. *Appl. Clay Sci.* **2016**, *119*, 348.
41. Maiti, M.; Bhowmick, A. K. *Polymer* **2006**, *47*, 6156.
42. Dubey, K. A.; Bhardwaj, Y. K.; Chaudhari, C. V.; Sabharwal, S. *J. Appl. Polym. Sci.* **2006**, *99*, 3638.
43. Maria, H. J.; Lyczko, N.; Nzihou, A.; Mathew, C.; George, S. C.; Joseph, K.; Thomas, S. *J. Mater. Sci.* **2013**, *48*, 5373.
44. Avalos, F.; Ortiz, J. C.; Zitzumbo, R.; Lopez-Manchado, M. A.; Verdejo, R.; Arroyo, M. *Eur. Polym. J.* **2008**, *44*, 3108.
45. Hakim, R. N.; Ismail, H. *J. Phys. Sci.* **2009**, *20*, 37.
46. Hakim, R. N.; Ismail, H. *Polym. Plast. Technol. Eng.* **2009**, *48*, 910.
47. López-Manchado, M. A.; Arroyo, M.; Herrero, B.; Biagiotti, J. (2003). *J. Appl. Polym. Sci.* **2003**, *89*, 1.
48. Teh, P. L.; Mohd Ishak, Z. A.; Hashim, A. S.; Karger-Kocsis, J.; Ishiaku, U. S. *J. Appl. Polym. Sci.* **2006**, *100*, 1083.
49. Varghese, S.; Karger-Kocsis, J. (2004). *J. Appl. Polym. Sci.* **2004**, *91*, 813.
50. Ali, Z.; El-Nemr, K.; Youssef, H.; Bekhit, M. *Polym. Compos.* **2013**, *34*, 1600.
51. Gatos, K. G.; Karger-Kocsis, J. *Eur. Polym. J.* **2007**, *43*, 1097.
52. Heinrich, G. Advanced Rubber Composites; Springer Science & Business Media: New York, **2011**, Vol. *239*, p 300.
53. Pokharel, P.; Pant, B.; Pokhrel, K.; Pant, H. R.; Lim, J. G.; Kim, H. Y.; Choi, S. *Composites Part B* **2015**, *78*, 192.
54. Chaudhari, C. V.; Dubey, K. A.; Bhardwaj, Y. K.; Sabharwal, S. *J. Macromol. Sci. Part B* **2012**, *51*, 839.
55. Pradhan, S.; Costa, F. R.; Wagenknecht, U.; Jehnichen, D.; Bhowmick, A. K.; Heinrich, G. *Eur. Polym. J.* **2008**, *44*, 3122.
56. Rajasekar, R.; Pal, K.; Heinrich, G.; Das, A.; Das, C. K. *Mater. Des.* **2009**, *30*, 3839.
57. Sadeghi Ghari, H.; Jalali-Arani, A.; Shakouri, Z. *Rubber Chem. Technol.* **2013**, *86*, 330.